SAE International™

High-Speed Microscopic Imaging of the Initial Stage of Diesel Spray Formation and Primary Breakup

2010-01-2247
Published
10/25/2010

Cyril Crua, Tenzin Shoba and Morgan Heikal
University of Brighton

Martin Gold and Cassandra Higham
BP Global Fuels Technology

ABSTRACT

The formation and breakup of diesel sprays was investigated experimentally on a common rail diesel injector using a long range microscope. The objectives were to further the fundamental understanding of the processes involved in the initial stage of diesel spray formation.

Tests were conducted at atmospheric conditions and on a rapid compression machine with motored in-cylinder peak pressures up to 8 MPa, and injection pressures up to 160 MPa. The light source and long range imaging optics were optimised to produce blur-free shadowgraphic images of sprays with a resolution of 0.6 µm per pixel, and a viewing region of 768×614 µm. Such fine spatial and temporal resolutions allowed the observation of previously unreported shearing instabilities and stagnation point on the tip of diesel jets. The tip of the fuel jet was seen to take the shape of an oblate spheroidal cap immediately after leaving the nozzle, due to the combination of transverse expansion of the jet and the physical properties of the fuel. The spheroidal cap was found to consist of residual fuel trapped in the injector hole after the end of the injection process. The formation of fuel ligaments close to the orifice was also observed, ligaments which were subsequently seen to breakup into droplets through hydrodynamic and capillary instabilities.

An ultra-high speed camera was then used to capture the dynamics of the early spray formation and primary breakup with fine temporal and spatial resolutions. The frame rate was up to 5 million images per second and exposure time down to 20 ns, with a fixed resolution of 1280×960 pixels covering a viewing region of 995×746 µm. A vortex ring motion within the vapourised spheroidal cap was identified, and resulted in a slipstream effect which led to a central ligament being propelled ahead of the liquid jet.

INTRODUCTION

The importance of the problem of spray breakup for various applications is well recognized and has been extensively studied experimentally and theoretically [1, 2, 3, 4, 5, 6, 7, 8, 9]. A rigorous theory of spray breakup would be very complex as it would need to involve modelling of nozzle flow, cavitation, instabilities, the initial formation of ligaments and droplets and their subsequent breakup, evaporation, the entrainment of air and the effects of turbulence [4]. Experimental characterization of the initial stage of diesel jet formation and primary breakup under realistic engine conditions is challenging due to the harsh environment in which they take place. This inherent complexity is compounded by the highly transient nature of the processes involved, along with the elevated velocities and the microscopic scale at which they occur. Direct visualisation techniques are invaluable to improve the fundamental understanding of primary breakup but because of the challenges posed by the conditions under which diesel jets occur, simplified experiments are often used to infer breakup characteristics at normal operating conditions. In particular, the injection and gas pressures are often reduced, the injector geometry simplified, and the fuel replaced by a more convenient fluid.

Microscopic imaging experiments of diesel sprays have been reported in the literature [e.g. 6, 13, 14, 15, 16], although with varying degrees in the quality of the images produced. Satisfactory lighting can be particularly difficult to obtain at microscopic level. High-power short duration laser pulses may seem appropriate, but speckle patterns caused by the

combined reflections of such monochromatic light conceal the underlying morphology of the spray, thus significantly degrading the quality of the resulting images and making their interpretation limited. Such optical artifacts can be observed in images recorded by Lai et al. [14], Badock et al. [16] and Heimgärtner & Leipertz [6], for example. Speckle patterns can be avoided by using a spark light instead of a laser, but the duration of the spark flashes are significantly longer and lead to motion blurring, even at low spray velocities, unless the exposure can be accurately controlled by the imaging device. The relatively long and random jitter associated with the timing of the spark can also lead to a significant proportion of 'missed' acquisitions which, combined with the long recharge time of the high-voltage electronics, may significantly lengthen the experimental work.

High quality shadowgraphic photographs of diesel sprays were obtained by spectrally diffusing a high-power laser pulse. These still images provided high resolution blur-free observations of the injection process at a microscopic scale. However, the value of these images can be limited due to the nature of still imaging and technical limitations of the injector. An additional issue associated with still imaging is the inherent lack of information on the spatiotemporal evolution of the transient jet and droplets observed. Specifically, there is no information on the velocity field, a quantity which is of particular significance for the investigation of breakup and essential for the approximation of relevant parameters such as the Weber and Reynolds numbers. In order to complement the fine spatial information derived from the still images, an ultra high speed camera was then used to accurately record the temporal evolution of diesel sprays at microscopic scales, with a second high speed camera simultaneously recording the macroscopic evolution of the complete spray. This allowed a precise tracking of the temporal evolution of diesel jets from the actual start of fuel delivery, thus eliminating the timing uncertainty associated with single images. This is particularly relevant when the transient jets being observed evolve over a shorter timescale than the mechanical and hydraulic jitters associated with solenoid-actuated servo-valve diesel injectors.

EXPERIMENTAL SETUP

RAPID COMPRESSION MACHINE

The experiments were carried out using a reciprocating rapid compression machine (RCM) based around a Ricardo Proteus single cylinder engine converted to liner ported, 2 stroke cycle operation [11]. The removal of the valve train allowed the fitting of an optical chamber of 80 mm in height and 50 mm diameter into the cylinder head. The optical access to the combustion chamber was provided by three removable sapphire glass windows. Due to the increased volume of the combustion chamber the compression ratio was reduced to 9:1. To simulate a real diesel engine with a compression ratio of 19:1, the intake air was conditioned to give in-cylinder pressures and temperatures up to 8 MPa and 540 K, respectively. For the present experiments the peak in-cylinder temperature was intentionally kept low in order to inhibit autoignition. Prior to motoring the RCM, the cylinder head was heated by a water jacket to 85°C and immersion heaters heated the oil to 40°C. The RCM was motored by a dynamometer to 500 rpm, and kept at stable in-cylinder conditions for the duration of the recordings.

The test conditions are summarised in Table 1, including the in-cylinder motored peak pressure, gas temperature and injection pressure. For each condition, microscopic images were recorded at a range of locations within the spray.

Table 1. Test conditions.

ICP (MPa)	Gas T. (K)	Density (kg/m^3)	Inj. P. (MPa)
0.1 (atm)	293	1.2	40,100
4	540	26	40,100,160
8	540	52	40,100,160

FUEL INJECTION EQUIPMENT

The fuel was delivered by a Delphi common-rail system, comprising a DFP-3 high-pressure pump rated at 2000 bar, and a seven hole DFI-1.3 injector with a VCO type nozzle. The high-pressure rail and the delivery pipe were both instrumented with pressure transducers. The rail pressure, timing and duration of the injection were independently controlled by a custom-built fuel injection controller. The nozzle's orifices were cylindrical with a diameter of 135 μm and a length of 1 mm. The nozzle had an equivalent cone angle of 154°, and the injector was mounted horizontally relative to the cameras. This injector was extensively characterised on a macroscopic scale by high-speed video and laser diagnostics [12]. Since all images were captured before the end of the injection event, it wasn't necessary to control the total mass of injected fuel. Instead, an injector trigger pulse with a fixed duration of 550 μs was used for all conditions.

The fuel used was an ultra-low sulphur reference fuel representative of automotive diesel with properties listed in Table 2.

Table 2. Diesel fuel properties.

Viscosity (at 40°C)	3.26	mm^2/s
Density (at 15°C)	834.4	kg/m^3
Surface tension	30	mN/m
Lubricity	500	µm (wsd)
Cetane index	55.3	
Sulphur content	< 0.5	mg/kg
PAH content	4.2	% (m/m)
FAME content	< 0.5	% (v/v)

OPTICAL SETUP

STILL IMAGING

The light source used for still imaging conditions was a frequency-doubled Nd:YAG laser, with a pulse duration of 7 ns. The light pulse was spectrally diffused by fluorescence and spatially expanded from 8 mm to 100 mm in order to provide homogeneous illumination over a sufficiently large area. Two high performance cooled digital 12 bit CCD cameras were used to simultaneously visualise the sprays at the microscopic and macroscopic scales. The camera facing the light source was fitted with a long range microscope with a 12 cm working distance, and optics were selected to obtain a magnification factor of 10.8 at the CCD sensor plane. Hence the resolution was 0.6 µm per pixel, and the viewing region of 768×614 µm. The second CCD camera was located orthogonally to the light source and provided a simultaneous macroscopic view of the 7 sprays.

Images were recorded for 44 different spatial locations covering the initial stages of spray formation, the evolution of the spray boundary at the tip and at the periphery of the jet, as well as the internal region where the transition from liquid jet to atomised spray occurs.

HIGH-SPEED VIDEO

In order to record the velocity of the sprays and to observe their transient behaviour, the CCD cameras were replaced by two high-speed video cameras. The optical setup used for the high-speed video recordings is shown in Figure 1. The intensified ultra high speed camera was capable of recording 16 images with an equivalent acquisition rate of up to 200 million frames per second, at a fixed resolution of 1280×960 pixels with 12 bit dynamic range. It was fitted with the long range microscope, resulting in an effective viewing region of 995×746 µm. This ultra high speed camera faced the light source, hence producing shadowgraphic images of the diesel sprays. The exposure time was adjusted between 20 ns and 200 ns in order to minimise motion blurring. Some blurring still occasionally occurred as a result of the shallow depth of field (approx. 100 µm) combined with the relative movement between the ultra high speed camera and the RCM.

A second high-speed camera was located orthogonally to the light source and recorded the full evolution of the spray on a macroscopic scale simultaneously to the ultra high speed camera. Its acquisition speed was set to 94,500 images per second, with a resolution of 24×192 pixels and a viewing region of 5×35 mm. This second camera was used to measure the evolution of spray penetration with time.

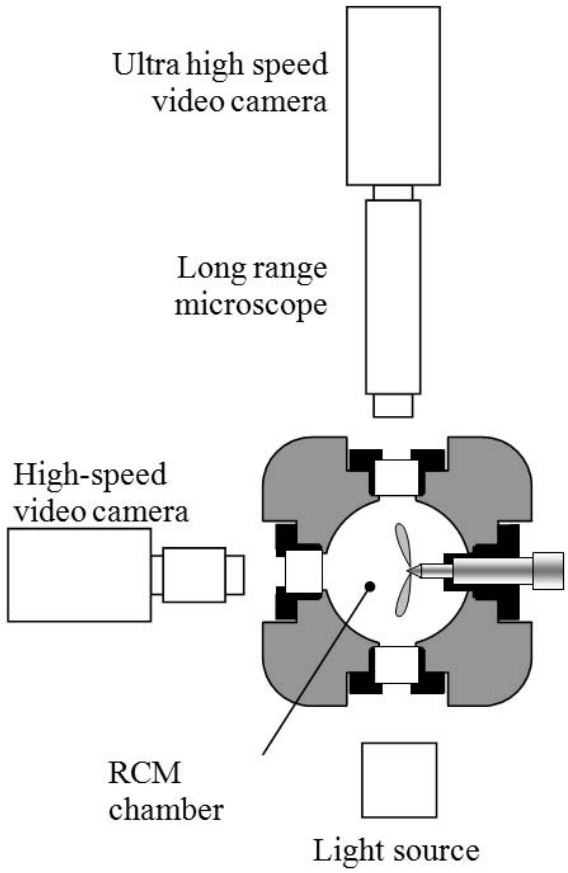

Figure 1. Optical setup for the simultaneous microscopic and macroscopic video recording of diesel sprays.

For the video recordings, the illumination of the sprays was achieved by a 500 joule xenon flashgun which delivered a 2 ms light pulse. This duration was sufficiently long to allow the recording of the complete injection event by the macroscopic camera, and bright enough to achieve exposures of 20 ns with the microscopic camera.

RESULTS AND DISCUSSION

INITIAL JET FORMATION

Figure 2 shows the evolution of diesel jets at non-evaporating conditions for injection pressures of 40 and 100 MPa. The images were rotated so that the nozzle orifice being observed in Fig. 2 lies horizontally. Timings are relative to the start of injection trigger pulse. The jets observed in Fig. 2 evolved over a shorter timescale than the mechanical and hydraulic

jitters associated with the injector, hence timings for individual images cannot be resolved. In Fig. 2a the emerging liquid fuel takes the shape of an undisrupted oblate spheroid. The transverse expansion of the jet is quite noticeable and explanations for this behaviour which were considered, but discarded, included the presence of cavitation bubbles within the jet, the aerodynamic interaction with the gas, and the slight compressibility of diesel fuel. The effect of gravity on the shape of the jet is intuitively ruled out, and this can easily be confirmed by calculating the capillary length, defined as $\sqrt{\sigma/\rho g}$. At the temperatures and pressures used in this investigation, capillary length for diesel fuel is between 1 and 1.9 mm. Since the characteristic lengths for this experiment are well below this value, it is safe to assume that gravitational forces have no influence on the shape of the initial fuel jet. The possible presence of cavitation bubbles within the jet was rebutted by the fact that cavitation is unlikely to be established at such an early stage of the injection process, and that no signs of gaseous bubbles were detected in the subsequent images and videos. For example in Fig. 2b the head of the mushroom-like jet, as observed and described by Badock et al. [16], is evidently free of gas as any internal impurities would be clearly observed there. The aerodynamic interaction with the gas, potentially inducing a deceleration of the tip of the liquid fuel and a transverse expansion can be ruled out due to the low density of the surrounding gas at ambient conditions, giving a liquid-gas density ratio of 695. The compressibility of diesel fuel is rather small and can be neglected as the volumetric expansion associated with a 40 MPa pressure drop at the nozzle exit is less than 2%. The transverse expansion of the jet in Fig. 2a can be explained by the initial acceleration of the injected fuel during the needle lift, and the laminar flow condition observed at the nozzle exit. In that respect, the transverse expansion is an indication of the spheroidal drop being inflated by the upstream fuel.

Ultra high speed videos indicated that for these conditions the fuel emerged from the nozzle orifice with a velocity of 16 m.s^{-1}. This relatively low initial velocity implies that the surface tension forces at the nozzle exit may not be insignificant compared to the inertial forces, at least at the early stage of injection. The balance of inertial and surface tension forces is defined by the Weber number, which can be calculated in the present case using the gas and liquid densities:

$$\mathrm{We_G} = \frac{\rho_g v^2 d}{\sigma} \text{ and } \mathrm{We_L} = \frac{\rho_l v^2 d}{\sigma}$$

with ρ_g the density of the gas (1.2 kg.m^{-3}), ρ_l the density of the fuel, v the exit velocity of the fuel (16 m.s^{-1}), d the orifice diameter (135 µm) and σ the surface tension of the fuel, giving $\mathrm{We_G}$ = 1.4 and $\mathrm{We_L}$ = 961. Using the kinematic viscosity in Table 2 the Reynolds number can be calculated for these conditions as 662. These values support the assumption that the jet in Fig. 2a is laminar and the observation that it is not inclined to breakup. In contrast, the 100 MPa jets in Fig. 2e-h appear to be turbulent and partially atomised. This agrees with a measured average tip velocity of approximately 100 m.s^{-1}, and the correspondingly higher $\mathrm{We_G}$ (~54), $\mathrm{We_L}$ (~37530) and Re (~4139) which indicate that the flow is both in a breakup regime and turbulent.

In effect, the transverse expansion of the jet was often sufficient in magnitude for the oblate spheroid to stick to the nozzle surface with a large contact angle, similarly to a sessile drop resting on a hydrophobic surface. It should be noted that the inertial forces are small but not negligible, and can be assumed to be responsible for the apparent large contact angle between the liquid fuel and the nozzle surface. As the injection velocity increases, the inertial forces become sufficient to detach the fuel droplet from the nozzle surface. This can be seen in Fig. 2b where the tip of the fuel jet takes the shape of a spheroidal cap, with its base still parallel to the nozzle surface. The striations of the jet leading to the spherical cap are likely to be a sign of the stretching caused by the sudden detachment of the cap from the nozzle. Tests conducted on the RCM at in-cylinder pressures (ICP) of 0.1, 4, 6 and 8 MPa showed that these structures are much more recurrent as the ICP was increased, indicating that the increased density of the surrounding gas slows down the penetration of the jet, thus further promoting a transverse expansion. Similar images were obtained by Badock et al. [16] with a single-hole injector, for an injection pressure of 25 MPa and gas pressure of 1.5 MPa, and described as stochastic mushroom-like structures. It is now evident that the spheroidal caps observed by Badock et al. and in Fig. 2 are formed by the combination of transverse jet expansion and are function of the physical properties of the fuel.

A stagnation point can be seen on the tip of this spheroidal cap (Fig. 2b), where the liquid boundary meets the horizontal axis of symmetry of the nozzle orifice. Ripples can be observed surrounding the stagnation point on the interface of the cap, which are possibly caused by shearing instabilities at the boundary between the liquid and gas interface. The wavelength associated with these surface ripples ranged between 3 and 8 µm and are proposed to be the result of a short-lived Kelvin-Helmholtz type instability. The occurrence of these interfacial disturbances indicates that a shear layer on the liquid side of the interface is also likely to exist. The ripples are especially noticeable on the lower liquid boundary in Fig. 2b, and appear to be oriented perpendicularly to the shear. This, in turn, would suggest the presence of a toroidal internal motion within the spheroidal cap. The outer surface of the cap rapidly becomes unstable and starts disintegrating (Fig. 2d), eventually leading to the formation of ligaments which break up into droplets through hydrodynamic and capillary instabilities. The disintegration of the cap does not result from the aforementioned Kelvin-Helmholtz ripples, but

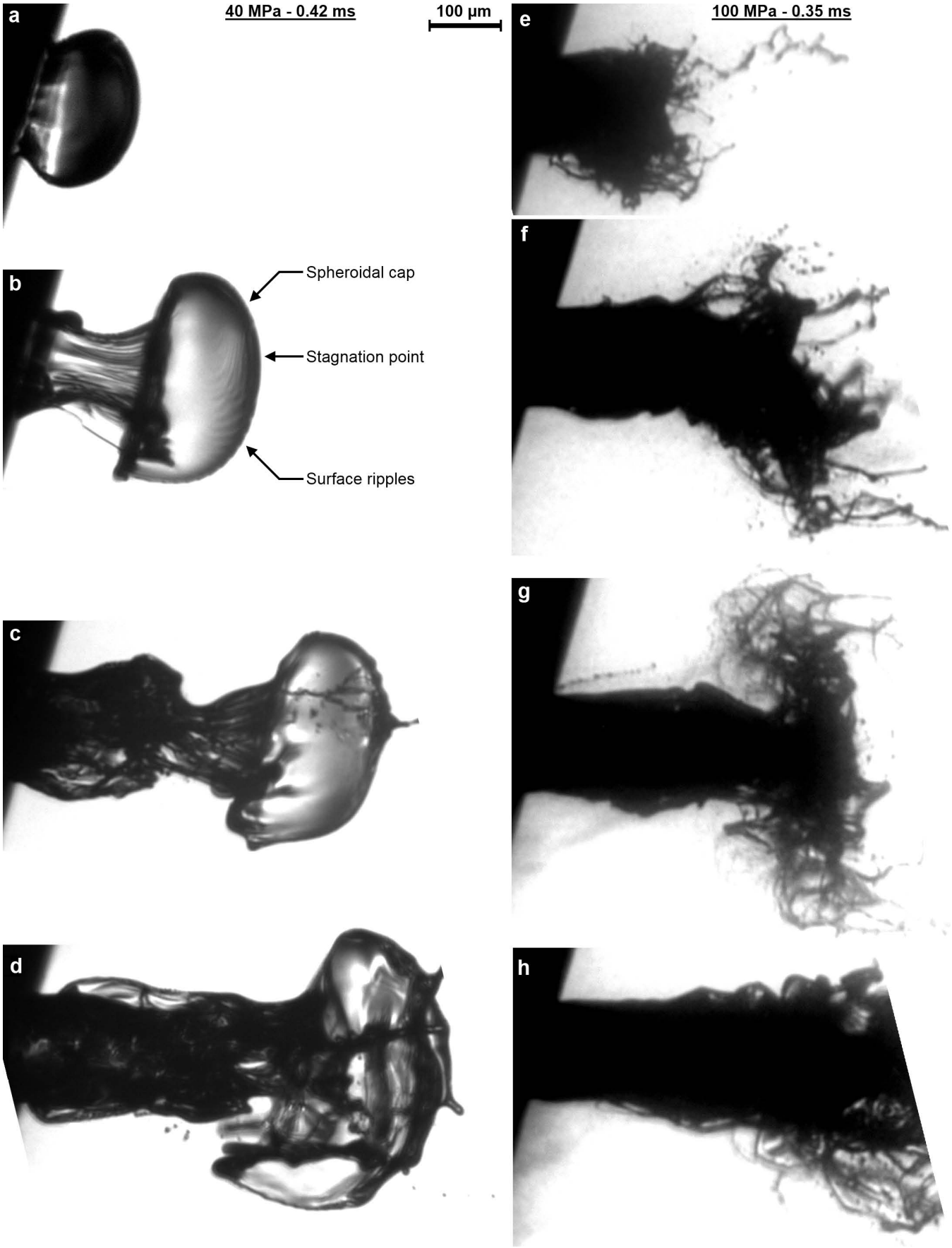

Figure 2. Effect of injection pressure on the initial stage of fuel injection at atmospheric conditions.

from the presence of a faster internal jet within the spheroidal cap. The evidence leading to this conclusion will be discussed next.

Figure 3 shows a series of images selected from a sixteen frame video recorded at evaporating conditions, where the interaction between the spheroidal cap and the jet that follows can be observed. Although still apparent, the spheroidal cap is much less distinguishable than at evaporating conditions. Further investigations led to the conclusion that at elevated in-cylinder temperatures the spheroidal cap is in vapour state, and can be observed due to the refraction of the light caused by density gradients. This effect offers the benefit of allowing the distinction to be made between the spheroidal cap and the jet that penetrates it, a distinction which cannot be made under non evaporating conditions such as in Fig. 2. The jet that forces the cap to detach from the nozzle surface in Fig. 3b-d is opaque indicating that it is in liquid state, while the spheroidal cap is already vapourised. Consequently, it is argued that the spheroidal cap consists of residual fuel from the previous injection, which was trapped in the nozzle orifice. The volume of the cap was approximated from the images by assuming axial symmetry, and was found to represent between 50% and 83% of the orifice's volume. This confirms that the volume of fuel that makes up the spheroidal cap can exist as trapped fuel in the orifice of the nozzle. The possibility of fuel being stored in the injector holes after the end of the injection process has been discussed in [20] and [21], and is believed to contribute to the formation of deposits in the nozzle orifices.

A thin ligament is formed in Fig. 3c on the tip of the liquid jet, within the spheroidal cap. This central ligament stretches ahead of the main jet and can be seen to perforate the cap in Fig. 3d. The formation of this thin ligament indicates that the velocity ahead of the tip of the jet, on the axis of symmetry, is significantly higher than on the periphery of the jet. This leads to the conclusion that the internal motion of the vapourised spheroidal cap must be toroidal in nature, thus corroborating the hypothesis made previously based on the observation of ripples on the surface of the liquid cap. The vortex ring motion within the vapourised fuel resulted in a slipstream effect which led to a thin central ligament being propelled ahead of the liquid jet.

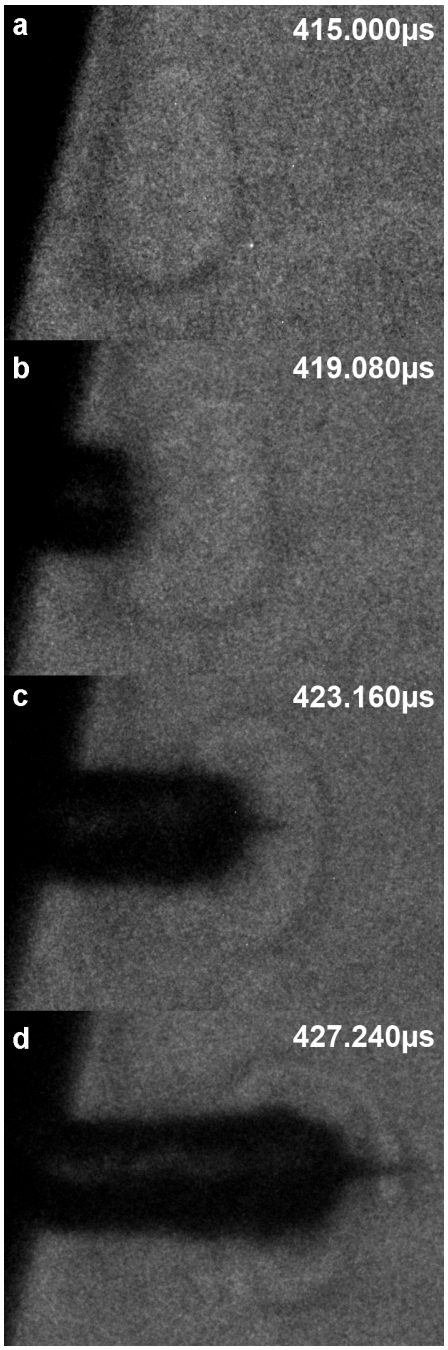

Figure 3. Perforation of the vapourised spheroidal cap by a liquid jet, indicating the presence of a vortex ring structure inside the cap. A central ligament is formed and propelled ahead of the main jet. P_{inj} = 40 MPa; ICP = 4 MPa. Timings are relative to start of injection trigger pulse.

Figure 4 shows the same process recorded by high-resolution still imaging, with a central ligament visibly propelled ahead of the jet as a result of the vortex ring motion in the spheroidal cap. The diameter of the ligament was measured to be 23 µm in this instance. It can also be observed that the jet

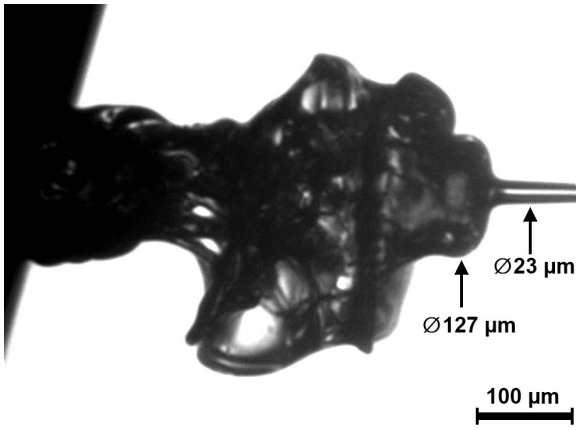

Figure 4. 23 µm central ligament propelled ahead of the jet by the vortex ring motion in the spheroidal cap. The jet seen in Fig. 3d ***at the base of the ligament is also visible here with a diameter of 127 µm. P_{inj} = 40 MPa; ICP = 0.1 MPa.***

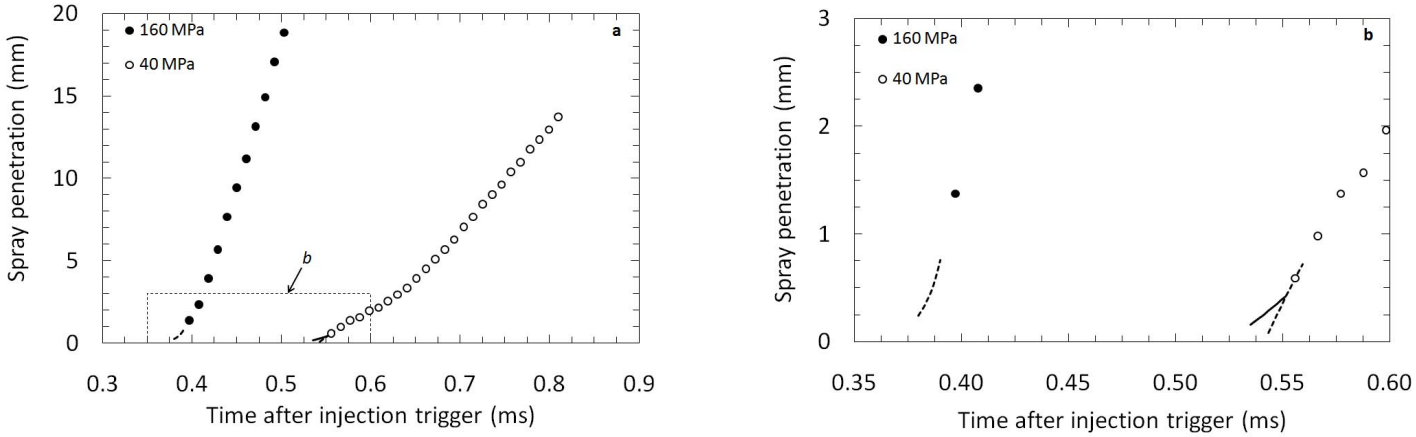

Figure 5. Evolution of liquid spray penetration with time for 0.1 MPa ICP (atmospheric condition) and two injection pressures, recorded at macroscopic (a) and microscopic (b) scales simultaneously. Solid lines represent the spheroidal cap's penetration, and the dotted lines the liquid jet's.

seen in Fig. 3d at the base of the ligament is also visible in Fig. 4 with a diameter of 127 µm. The jet appears to have just perforated the tip of the spheroidal cap, and thereby created a short corolla whose rim can be seen on the surface of the spheroidal cap. Similar corollas can seen in Fig. 2d and, albeit less noticeably, in Fig. 3d.

This vortex ring motion is believed to justify previously unexplained observations made by Badock et al. [16] and Roisman et al. [17] of central ligaments present downstream of diesel sprays.

INFLUENCE OF OPERATING CONDITIONS

Figures 5 and 6 show the effect of injection pressure on the evolution of liquid spray penetration with time, obtained from the simultaneous video recording of single spray events at macroscopic and microscopic scales. Tip penetration measurements were obtained from every frame of the microscopic ultra high speed videos, both for the spheroidal cap and the subsequent jet. In Figs. 5, 6 and 7 the solid lines represent the penetration of the cap, while the dotted lines represent the penetration of the jet. Once the jet has overtaken the cap, as in Fig. 3d for example, only the jet's penetration is plotted as the cap breaks up into ligaments and droplets.

The macroscopic evolutions follow the well documented two stage spray penetration profile [18, 19]. The first stage is a linear evolution of spray penetration with time, which can be observed on Fig. 6a between 0.38 and 0.45 ms for 160 MPa injection pressure. During the second stage, from 0.45 ms onward in Fig. 6a for 160 MPa, the spray tip velocity reduces and the penetration follows a square-root temporal dependence.

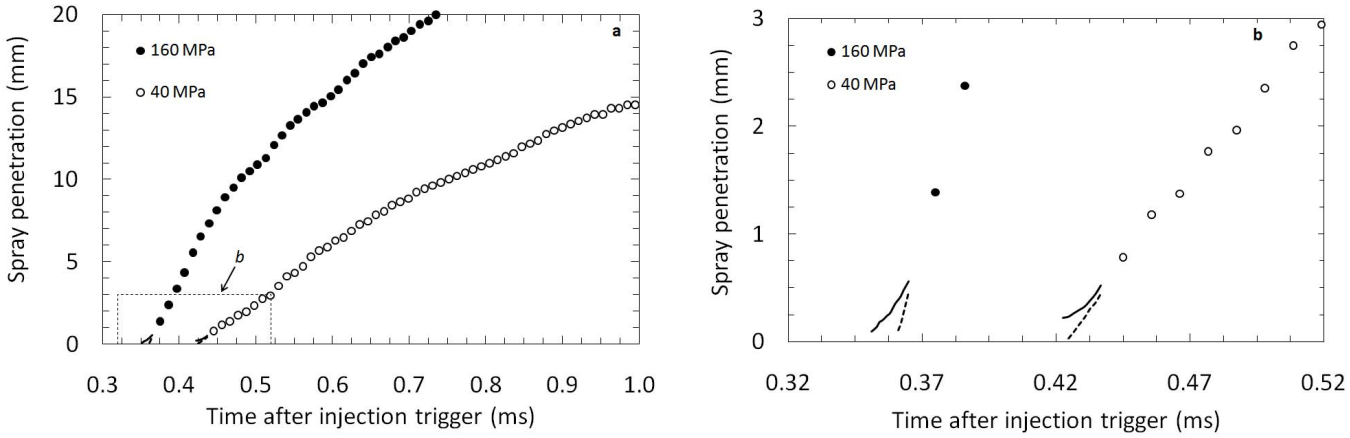

Figure 6. Evolution of liquid spray penetration with time for 4 MPa ICP, recorded at macroscopic (a) and microscopic (b) scales simultaneously. Solid lines represent the spheroidal cap's penetration, and the dotted lines the liquid jet's.

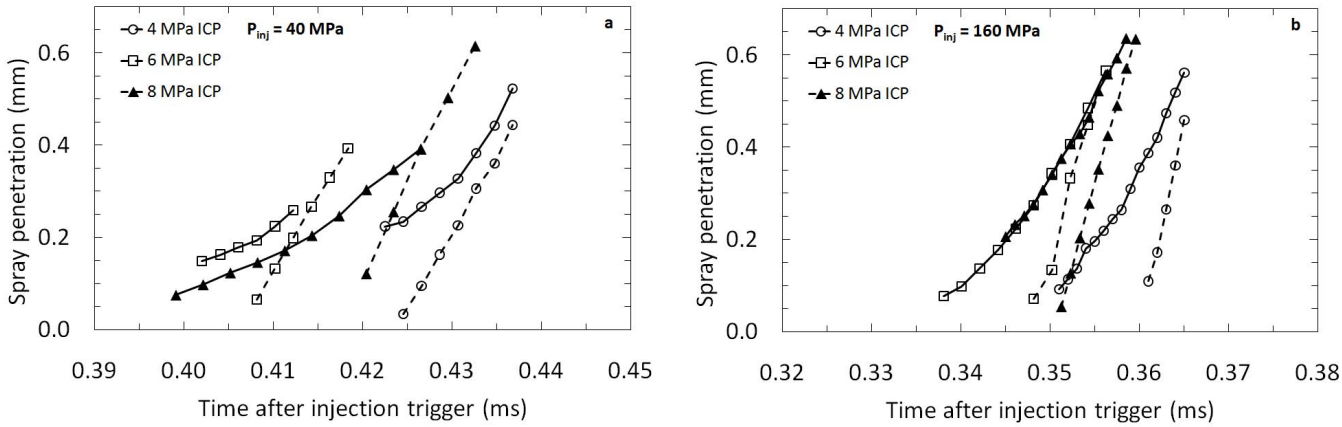

Figure 7. Initial spray penetration for 40 (a) and 160 MPa (b) injection pressure and a range of ICPs. Solid lines represent the vapourised spheroidal cap's penetration, and the dotted lines the liquid jet's.

Whereas the macroscopic measurements are in agreement with the literature, it is interesting to note that the microscopic scale observations indicate that the initial stage of fuel injection is more complex than the previously reported linear evolution. Indeed, while the microscopic jet follows the expected linear macroscopic evolution, to the best of the authors' knowledge the precursory spheroidal cap does not follow previously reported temporal trends. The cap grows at a noticeably slower rate than the subsequent jet, and represents a preliminary phase to the accepted two stage spray penetration profile. Most previous experiments failed to observe the spheroidal cap due to unrealistic operating conditions and the lack of sufficiently high spatial and temporal resolutions. While the liquid jet is opaque and observable by standard shadowgraphy, the spheroidal cap that precedes it is in vapour state and only visible when using optical diagnostics which are sensitive to density gradients. Badock et al. [16] used a suitable setup and reported the existence of this mushroom-like structure at non-evaporating conditions, without fully investigating its origin and temporal evolution, possibly dismissing it as a peculiarity resulting from their customised injector and working fluid.

The lifetime of the cap appears to be governed by the balance between kinetic and surface tension forces, which are primarily determined by the injection pressure and the fuel's physical properties. Higher injection pressures increase the kinematic energy of the injected fuel, and therefore lead to a shorter lifetime. From Fig. 7 the lifetime of the cap was estimated at 30 μs for 40 MPa and 20 μs for 160 MPa injection pressure. For the motored test conditions (4, 6 and 8 MPa ICP) the in-cylinder pressure had a negligible influence on the velocity and timing of the cap and jet.

SUMMARY

Simultaneous observations of diesel jets were conducted for a range of operating conditions at microscopic and macroscopic scale, using still imaging and ultra high speed video. These observations indicated that the initial stage of fuel injection is more complex than the accepted linear temporal evolution. An oblate spheroidal cap was observed for a wide range of conditions, and consists of residual fuel from the previous injection, which has been trapped in the nozzle orifice. These findings confirm that vapourised fuel does remain trapped in the injector holes after the end of the injection process, and would support the theory that the formation of deposits in the holes of diesel injector nozzles may be linked to the degradation of such residual fuel.

The influence of engine operating conditions on the spatiotemporal evolution of the spheroidal cap was described. Under non-evaporating conditions ripples were observed surrounding a stagnation point on the surface of the cap, possibly caused by shearing instabilities at the boundary between the liquid and gas interface. At evaporating conditions a vortex ring motion within the spheroidal cap was identified, and resulted in a slipstream effect which led to a central ligament being propelled ahead of the liquid jet.

REFERENCES

1. Som, S. and Aggarwal, S.K., "Effects of Primary Breakup Modeling on Spray and Combustion Characteristics of Compression Ignition Engines," *Combustion and Flame* **157**(6):1179-1193, 2010, doi:10.1016/j.combustflame.2010.02.018.

2. Dumouchel, C., "On the Experimental Investigation on Primary Atomization of Liquid Streams," *Experiments in Fluids* **45**(3):371-422, 2008, doi:10.1007/s00348-008-0526-0.

3. Eggers, J. and Villermaux, E., "Physics of Liquid Jets," *Reports on progress in physics* **71**(3):036601, 2008, doi:10.1088/0034-4885/71/3/036601.

4. Faeth, G., Hsiang, L. and Wu, P., "Structure and Breakup Properties of Sprays," *International Journal of Multiphase Flow* **21**(supp 1):99-127, 1995, doi:10.1016/0301-9322(95)00059-7.

5. Gorokhovski, M. and Herrmann, M., "Modeling Primary Atomization," *Annual Review of Fluid Mechanics* **40**(1):343-366, 2008, doi:10.1146/annurev.fluid.40.111406.102200.

6. Heimgärtner, C. and Leipertz, A., "Investigation of Primary Diesel Spray Breakup Close to the Nozzle of a Common Rail High Pressure Injection System," presented at 8th ICLASS, Pasadena, USA, July 2000.

7. Hossainpour, S. and Binesh, A., "Investigation of Fuel Spray Atomization in a Di Heavy-Duty Diesel Engine and Comparison of Various Spray Breakup Models," *Fuel* **88**(5):799-805, 2009, doi:10.1016/j.fuel.2008.10.036.

8. Lefebvre, A.H., Atomization and sprays, Hemisphere Publishing, New York, 1989.

9. Liu, Z., Im, K., Xie, X., Wang, Y., Zhang, X., Moon, S., Gao, J., Fezzaa, K., Lai, M. and Harkay, K., "Ultra-Fast Phase-Contrast X-Ray Imaging of near-Nozzle Velocity Field of High-Speed Diesel Fuel Sprays," presented at ILASS-Americas, Cincinnati, Ohio, USA, May 2010.

10. Reitz, R. and Diwakar, R., "Structure of High-Pressure Fuel Sprays," SAE Technical Paper 870598, 1987, doi:10.4271/870598.

11. Crua, C., "Combustion Processes in a Diesel Engine," Ph.D. thesis, University of Brighton, UK, 2002.

12. Karimi, K., "Characterisation of Multiple-Injection Diesel Sprays at Elevated Pressures and Temperatures," Ph.D. thesis, University of Brighton, UK, 2007.

13. Bae, C., Yu, J., Kang, J., Kong, J. and Lee, K., "Effect of Nozzle Geometry on the Common-Rail Diesel Spray," SAE Technical Paper 2002-01-1625, 2002, doi:10.4271/2002-01-1625.

14. Lai, M., Wang, T., Xie, X., Han, J., Henein, N., Schwarz, E. and Bryzik, W., "Microscopic Characterization of Diesel Sprays at VCO Nozzle Exit," SAE Technical Paper 982542, 1998, doi:10.4281/982542.

15. Sjöberg, H., Manneberg, G. and Cronhjort, A., "Long-Working-Distance Microscope Used for Diesel Injection Spray Imaging," *Optical Engineering* **35**(12):3591-3596, 1996, doi:10.1117/1.601113.

16. Badock, C., Wirth, R., Fath, A. and Leipertz, A., "Investigation of Cavitation in Real Size Diesel Injection Nozzles," *International Journal of Heat and Fluid Flow* **20**(5):538-544, 1999, doi:10.1016/S0142-727X(99)00043-0.

17. Roisman, I. V., Araneo, L. and Tropea, C., "Effect of Ambient Pressure on Penetration of a Diesel Spray," *International Journal of Multiphase Flow* **33**(8):904-920, 2007, doi:10.1016/j.ijmultiphaseflow.2007.01.004.

18. Hiroyasu, H. and Arai, M., "Structure of Fuel Sprays in Diesel Engines," SAE Technical Paper 900475, 1990, doi:10.4271/900475.

19. Naber, J. D. and Siebers, D. L., "Effects of Gas Density and Vaporization on Penetration and Dispersion of Diesel Sprays," SAE Technical Paper 960034, 1996, doi:10.4271/960034.

20. Lepperhoff, G. and Houben, M., "Mechanisms of Deposit Formation in Internal Combustion Engines and Heat Exchangers," SAE Technical Paper 931032, 1993, doi:10.4271/931032.

21. Birgel, A., Ladommatos, N., Aleiferis, P., Zuelch, S., Milovanovic, N., Lafon, V., Orlovic, A., Lacey, P. and Richards, P., "Deposit Formation in the Holes of Diesel Injector Nozzles: A Critical Review," SAE Technical Paper 2008-01-2383, 2008, doi:10.4271/2008-01-2383.

CONTACT INFORMATION

Correspondence should be addressed to Dr Cyril Crua: C.Crua@brighton.ac.uk. Full contact details can be found on www.brighton.ac.uk/shrl/crua.

ACKNOWLEDGEMENTS

The authors would like to thank BP Global Fuels Technology and the EPSRC (CASE 07000437) for financial support. The EPSRC Engineering Instrument Pool is acknowledged for supplying equipments. The authors are also grateful to Mr. Rousselet and Mr. Geneix for their contributions to the experiments.

DEFINITIONS/ABBREVIATIONS

σ
Surface tension

ρ
Density

g
Acceleration due to gravity

VCO
Valve-Covered Orifice

ICP
In-Cylinder Pressure

RCM
Rapid Compression Machine

The Engineering Meetings Board has approved this paper for publication. It has successfully completed SAE's peer review process under the supervision of the session organizer. This process requires a minimum of three (3) reviews by industry experts.

ISSN 0148-7191

doi:10.4271/2010-01-2247

SAE Customer Service:
Tel: 877-606-7323 (inside USA and Canada)
Tel: 724-776-4970 (outside USA)
Fax: 724-776-0790
Email: CustomerService@sae.org
SAE Web Address: http://www.sae.org
Printed in USA